





Conference Report

# Anisotropic Flow Measurements of Identified Hadrons with MPD Detector at NICA

Petr Parfenov <sup>1,\*</sup> , Dim Idrisov <sup>1</sup> , Vinh Ba Luong <sup>1</sup> , Nikolay Geraksiev <sup>2,3</sup> , Anton Truttse <sup>1</sup> and Alexander Demanov <sup>1</sup>

<sup>1</sup> Physics of Condensed Matter Department, NESPI, National Research Nuclear University (Moscow Engineering Physics Institute), Kashirskoe Highway 31, 115409 Moscow, Russia; DMIdrisov@mephi.ru (D.I.); lbavinh@gmail.com (V.B.L.); AATruttse@mephi.ru (A.T.); demanov1997@gmail.com (A.D.)

<sup>2</sup> FPET, Plovdiv University “Paisii Hilendarski”, “Tzar Assen” str. 24, 4000 Plovdiv, Bulgaria; geraksiev@jinr.ru

<sup>3</sup> VBLHEP, Joint Institute for Nuclear Research, Joliot-Curie str 6, 141980 Dubna, Russia

\* Correspondence: PEPArfenov@mephi.ru

**Abstract:** The primary scientific mission of the Multi-Purpose Detector (MPD) at the accelerator Nuclotron-based Ion Collider facility (NICA) (Dubna) is to investigate the properties of strongly interacting matter at high net-baryon densities. The goal of this work is to study the performance of the MPD detector for directed and elliptic flow measurements of identified hadrons by using the realistic Monte Carlo simulations of heavy-ion collisions at energies  $\sqrt{s_{NN}} = 4.5\text{--}11$  GeV.

**Keywords:** heavy-ion collisions; anisotropic flow; MPD experiment; NICA



**Citation:** Parfenov, P.; Idrisov, D.; Luong, V.B.; Geraksiev, N.; Truttse, A.; Demanov, A. Anisotropic Flow Measurements of Identified Hadrons with MPD Detector at NICA. *Particles* **2021**, *4*, 146–158. <https://doi.org/10.3390/particles4020014>

Academic Editor: Peter Senger

Received: 8 March 2021

Accepted: 22 March 2021

Published: 27 March 2021

**Publisher’s Note:** MDPI stays neutral with regard to jurisdictional claims in published maps and institutional affiliations.



**Copyright:** © 2021 by the authors. Licensee MDPI, Basel, Switzerland. This article is an open access article distributed under the terms and conditions of the Creative Commons Attribution (CC BY) license (<https://creativecommons.org/licenses/by/4.0/>).

## 1. Introduction

The Nuclotron-based Ion Collider facility (NICA) is under construction at the Joint Institute for Nuclear Research (JINR), Dubna, Russia. NICA will collide heavy-ions ( $^{198}\text{Au} + ^{198}\text{Au}$ ,  $^{209}\text{Bi} + ^{209}\text{Bi}$ ) at energies in the range of  $\sqrt{s_{NN}} = 4$  to 11 GeV per nucleon pair in the center-of-mass system to provide an opportunity of studying the matter in the region of high net-baryon density [1]. The Multi-Purpose Detector (MPD) experiment at NICA will measure various prominent diagnostic probes sensitive to the Equation-of-State (EOS) and transport properties of the strongly interacting matter [2,3]. Among them, the most prominent one is the azimuthal collective flow of the produced hadrons relative to the collision symmetry plane [4]. It can be quantified by Fourier coefficients  $v_n$  in the expansion of the particle azimuthal distribution as:

$$dN/d\phi \propto 1 + \sum_{n=1} 2v_n \cos(n(\phi - \Psi_n)), \quad (1)$$

where  $n$  is the order of the harmonic,  $\phi$  is the azimuthal angle of particle of the given type, and  $\Psi_n$  is the azimuthal angle of the  $n^{\text{th}}$  order symmetry plane. The  $n^{\text{th}}$  order flow coefficients  $v_n$  can be calculated as  $v_n = \langle \cos[n(\phi - \Psi_n)] \rangle$ , where the brackets denote the average over the particles and events. Directed ( $v_1$ ) and elliptic ( $v_2$ ) flows are the dominant flow signals and have been studied by experiments carried out at several facilities such as the Schwer-Ionen-Synchrotron (SIS), the Alternating Gradient Synchrotron (AGS), the Super Proton Synchrotron (SPS), the Relativistic Heavy-Ion Collider (RHIC) and the Large Hadron Collider (LHC) [4,5]. The collision energy dependence of flow coefficients is of particular importance. The  $v_1$  and  $v_2$  results from the STAR Beam Energy Scan program at RHIC [6–9], NA61/SHINE program at SPS [10], E895 program at AGS [11,12] and HADES program at SIS [13] have indicated strong energy dependence at NICA energies [14]. In this work, we discuss the anticipated performance of the MPD detector for differential anisotropic flow measurements of identified hadrons at NICA energies.

## 2. MPD Detector System and Simulation Setup

The MPD has been designed as a  $4\pi$  spectrometer for detecting charged hadrons, electrons and photons in heavy-ion collisions at high luminosity. In the first stage of operation in 2023, the MPD will consist of the Time Projection Chamber (TPC), the Time-of-Flight (TOF) detector, the electromagnetic calorimeter (ECal), the forward hadron calorimeter (FHCa) and the fast forward detector (FFD); see left panel of Figure 1. The TPC will provide 3D tracking of charged particles, as well as measuring the specific ionization energy loss  $dE/dx$  to identify the particles with  $|\eta| < 1.2$ . The TPC will be surrounded by a cylindrical barrel of the Time-of-Flight (TOF) detector. The TOF system of the MPD developed to identify the charged hadrons is based on the technology of Multigap Resistive Plate Chambers (MRPC). The detector is designed to provide both the time and coordinate measurements with the accuracy of the order of 80 ps and 0.5 cm, respectively. Two arms of hadron calorimeters (FHCa), made of 44 modules of lead-scintillator sampling calorimeters and covering the pseudorapidity range of  $2.0 < |\eta| < 5$ , will measure the forward going energy distribution. The information from FHCa about the energy deposit will be used to reconstruct the event plane, see right panel of Figure 1.

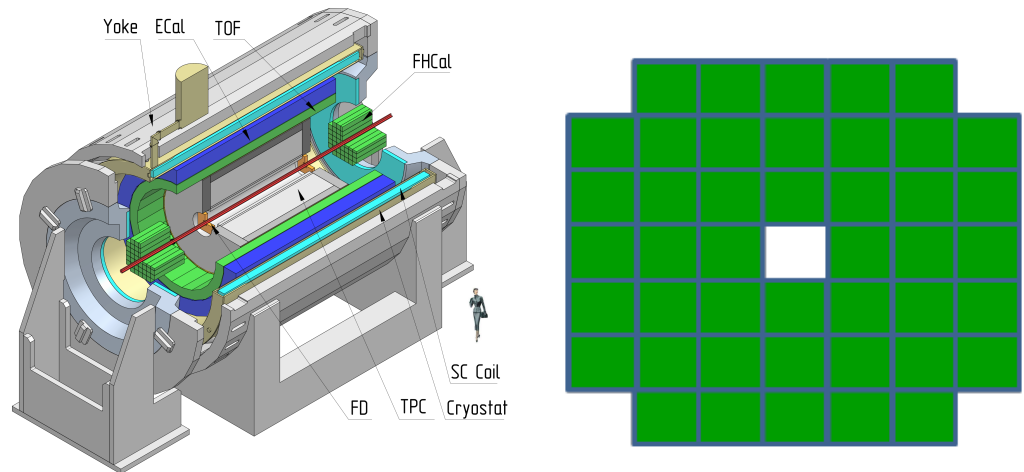


**Figure 1.** (left) The schematic view of the Multi-Purpose Detector (MPD) detector in Stage 1 (right). The module structure of the forward hadron calorimeter (FHCa) calorimeter (front view).

In this work, we used the cascade version of the Ultra-relativistic Quantum Molecular Dynamics (UrQMD) model (version 3.4) [15,16] to simulate the heavy-ion collisions at NICA energies:  $\sqrt{s_{NN}} = 4.5, 7.7$  and 11 GeV. In total, the sample of 100 M of minimum bias Au + Au and Bi + Bi events was used to analyze the directed and elliptic flow signals of the identified hadrons. We applied the term “true” for these  $v_1$  and  $v_2$  results, obtained from the direct analysis of the generated events. At the next step, the same sample of UrQMD minimum bias events was made as an input for the full chain of realistic simulations of the MPD detector subsystems based on the GEANT4 [17] platform and reconstruction algorithms built in the MPDROOT. The  $v_n$  results obtained from the flow analysis of these fully reconstructed events are termed as the “reco” data.

## 3. Analysis Procedure

The track reconstruction in MPD is based on the Kalman filter technique [18] and the minimal requirement of 16 TPC hits ensures a low momentum error. We introduced a 3D distance of the closest approach (DCA) between the track and the reconstructed primary vertex. The primary tracks were selected with the  $2\sigma$  cut on the DCA. The relative transverse momentum resolution ( $\Delta p_T/p_T$ ) for primary tracks as a function of  $p_T$  is shown in the left panel of Figure 2.  $\Delta p_T/p_T$  is less than 3% for tracks with  $0.1 < p_T < 1.8$  GeV/c and for the pseudorapidity range  $|\eta| < 1.5$ , see right panel of Figure 2. The resolution degrades rapidly above  $\eta = 1.5$  due to the decrease of the number of TPC space points [18].

The analysis was performed for tracks from the kinematic regions of TPC with the higher tracking efficiency:  $0.2 < p_T < 2.5$  GeV/c and  $|\eta| < 1.5$ .

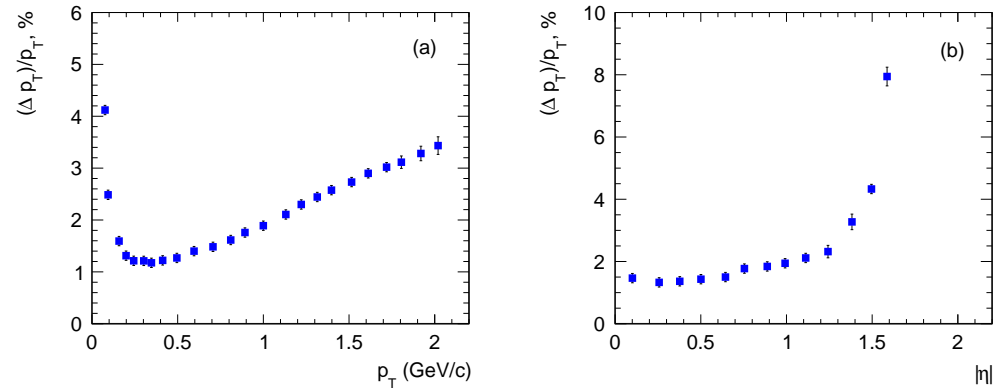


**Figure 2.** Relative transverse momentum resolution for primary tracks as a function of  $p_T$  (a) and pseudorapidity  $\eta$  (b).

The centrality classes are defined based on the uncorrected charged particle multiplicity ( $N_{ch}$ ) distribution in the TPC for pseudorapidity  $|\eta| < 0.5$  and full azimuth. As an example, Figure 3 shows the track multiplicity distribution for the Au + Au (left panel) and Bi + Bi (right panel) collisions at  $\sqrt{s_{NN}} = 7.7$  GeV compared to those from Monte Carlo (MC)–Glauber simulations (red line) [19]; 10% centrality classes are indicated with black vertical lines in the Figure 3.

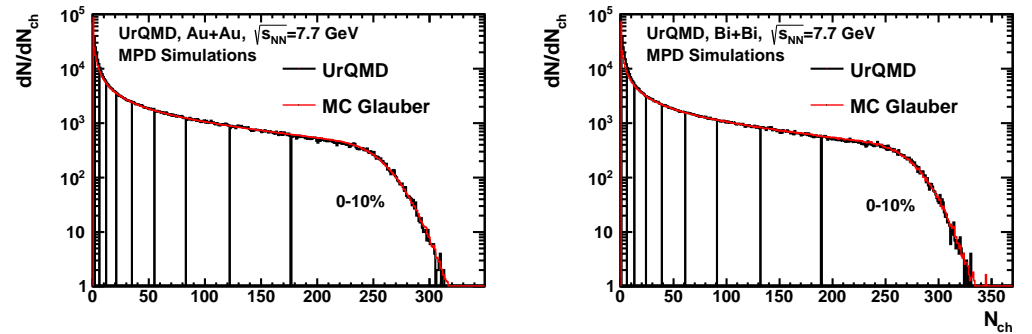


**Figure 3.** Track multiplicity distribution from the fully reconstructed Ultra-relativistic Quantum Molecular Dynamics (UrQMD) events for Au + Au (left panel) and Bi + Bi (right panel) collisions at  $\sqrt{s_{NN}} = 7.7$  GeV compared to the fitted distribution using Monte Carlo (MC)–Glauber approach (red line). The 10% centrality classes defined with MC–Glauber normalization are indicated with black vertical lines.

Identification of the charged hadrons in the MPD experiment is based on a combination of momentum information, the specific energy loss ( $dE/dx$ ) in the Time-Projection Chamber (TPC) and time-of-flight measurements from the TOF detector [18]. Time-of-flight measurements from the TOF detector were used in conjunction with the measured particle momentum and flight-path length to generate a mass-squared ( $m^2$ ) distribution, see left panel of Figure 4.

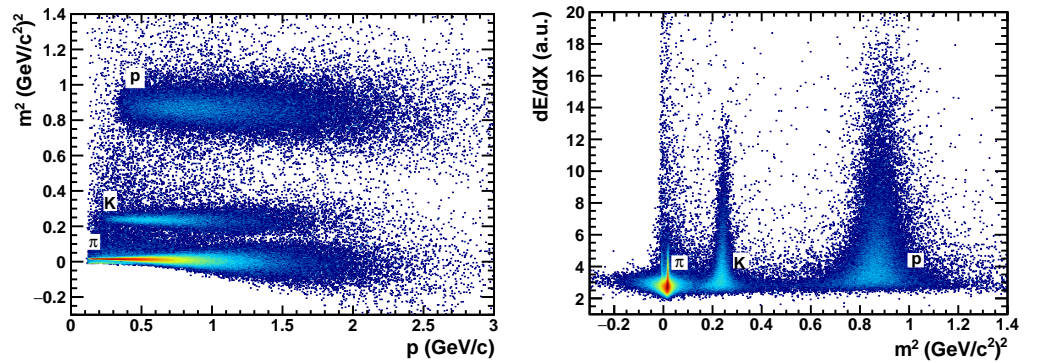


**Figure 4.** (left) Momentum dependence of mass-squared ( $m^2$ ) of charged particles. (right)  $dE/dx$  vs.  $m^2$  for combined system Time-Projection Chamber (TPC) + Time-of-Flight (TOF) for charged hadrons with momentum  $0 < p < 3$  GeV/c.

The identified candidates (hadrons and light nuclei) can be selected within the pre-defined elliptical ranges around a nominal position in  $dE/dx$  and  $m^2$  axes fixed for each type of particles, see right panel of Figure 4. The widths of these distributions provide an additional criterion of identification. Charged pions and kaons can be easily distinguished up to 1.5 GeV/c in transverse momentum, whereas at higher momenta, the particle species start to significantly overlap. Protons and mesons can be separated up to 2.5 GeV/c.

Short-lived weakly-decaying particles, such as  $K_S^0$  and  $\Lambda$ , have been reconstructed using the invariant mass technique. The combinatorial background from uncorrelated particles has been reduced by the selection criteria based on the topology of the specific decay. The topological information about the primary and secondary decay vertex positions, the distance of the closest approach (dca) of the daughter particles to the primary vertex, the dca of the mother particle to the primary vertex, and the dca between the daughter tracks have been obtained by the Kalman filtering algorithm based on the MpdParticle tool [20]. The cuts have been applied to optimize the signal of  $K_S^0$  and  $\Lambda$  particles. As an example, Figure 5 shows the invariant mass distributions for  $K_S^0$  (left panel) and  $\Lambda$  (right panel) particles with  $0.2 < p_T < 2.4$  GeV/c for 10–40% central Au + Au collisions at  $\sqrt{s_{NN}} = 11$  GeV.

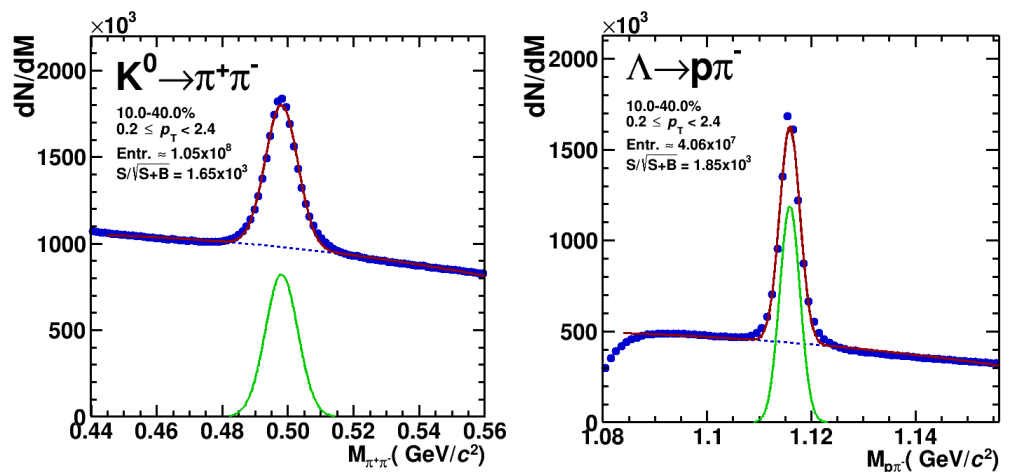


**Figure 5.** Invariant mass distributions for  $K_S^0$  (left panel) and  $\Lambda$  (right panel) particles for 10–40% central Au + Au collisions at  $\sqrt{s_{NN}} = 11$  GeV.

The event plane method is used to obtain the present results for the directed ( $v_1$ ) and elliptic ( $v_2$ ) flow coefficients of the produced particles. The event plane method correlates the azimuthal angle  $\varphi$  of each particle with the azimuthal angle  $\Psi_n$  of the event plane determined from the anisotropic flow itself [4,21]. Directed flow  $v_1$  is large at NICA

energies compared to other flow harmonics [14]. It is the strongest in the forward rapidity region (i.e., in FHCaI acceptance area:  $2 < |\eta| < 5$ ). For these reasons the first harmonic event plane  $\Psi_{1,\text{FHCaI}}$  is used to study the present flow performance. The event plane angle  $\Psi_{1,\text{FHCaI}}$  has been calculated from the energy deposition in a given module of the FHCaI by constructing the so-called flow Q-vector  $Q_{1,\text{FHCaI}}$  (two-dimensional vector in the transverse to the beam plane):

$$Q_{1,x} = \frac{\sum E_i \cos \varphi_i}{\sum E_i}, \quad Q_{1,y} = \frac{\sum E_i \sin \varphi_i}{\sum E_i}, \quad \Psi_{1,\text{FHCaI}} = \tan^{-1} \left( \frac{Q_{1,y}}{Q_{1,x}} \right), \quad (2)$$

where  $\varphi_i$  is the azimuthal angle of the center of the  $i^{\text{th}}$  FHCaI module in the transverse plane, and  $E_i$  is the energy deposition in the  $i^{\text{th}}$  module of FHCaI (weight to improve the event plane resolution). The weights  $E_i$  have opposite signs for backward and forward rapidities due to the anti-symmetry of the  $v_1$  as a function of rapidity  $y$ . The reconstructed  $\Psi_{1,\text{FHCaI}}$  can be used to measure the differential directed flow  $v_1^{\Psi_{1,\text{FHCaI}}}$  and elliptic  $v_2^{\Psi_{1,\text{FHCaI}}}$  flow coefficients of the produced particles detected in TPC ( $|\eta| < 1.5$ ).

$$v_n^{\Psi_{1,\text{FHCaI}}}(p_T, y, \text{centrality}) = \frac{\langle \cos(n(\phi - \Psi_{1,\text{FHCaI}})) \rangle}{R_n(\Psi_{1,\text{FHCaI}})}, \quad (3)$$

where  $R_n(\Psi_{1,\text{FHCaI}})$  represents the event plane resolution factor. The two-subevent method with extrapolation algorithm was applied to estimate the event plane resolution factors [21]. Figure 6 shows the centrality dependence of the event plane resolution factors  $R_n(\Psi_{1,\text{FHCaI}})$  for directed  $v_1$  (left panel) and elliptic  $v_2$  (right panel) flow measurements for Au + Au collisions at  $\sqrt{s_{NN}} = 4.5, 7.7$  and 11 GeV. For the mid-central Au + Au events at  $\sqrt{s_{NN}} = 11$  GeV the resolution factor is as high as 0.9—for  $v_1$  and 0.65—for  $v_2$  measurements. The event plane resolution degrades slowly while decreasing the collision energy.

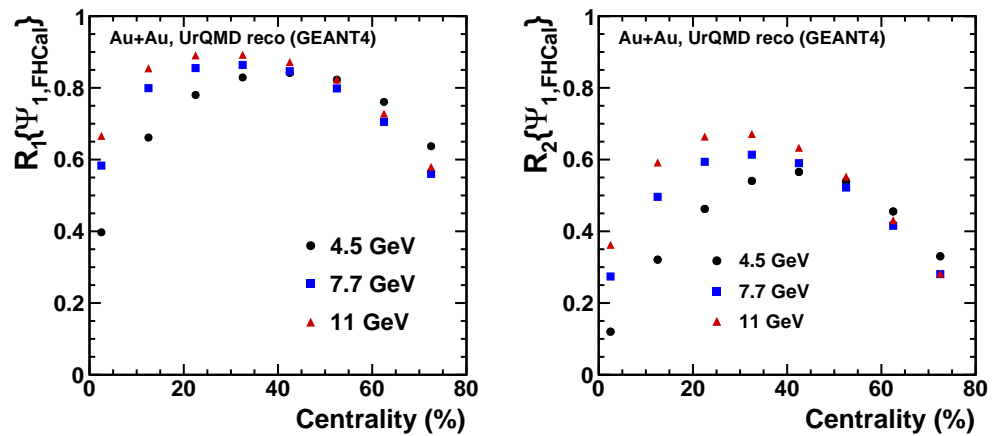


**Figure 6.** Centrality dependence of event plane resolution factors  $R_n(\Psi_{1,\text{FHCaI}})$  for the directed  $v_1$  (left) and elliptic  $v_2$  (right) flow measurements for Au + Au collisions at  $\sqrt{s_{NN}} = 4.5, 7.7$  and 11 GeV.

Figure 7 shows the comparison of the event plane resolution factors  $R_n(\Psi_{1,\text{FHCaI}})$  for the Au + Au (open symbols) and Bi + Bi (filled symbols) collisions at  $\sqrt{s_{NN}} = 7.7$  GeV. As expected they have very similar values for the same bins in the collision centrality.

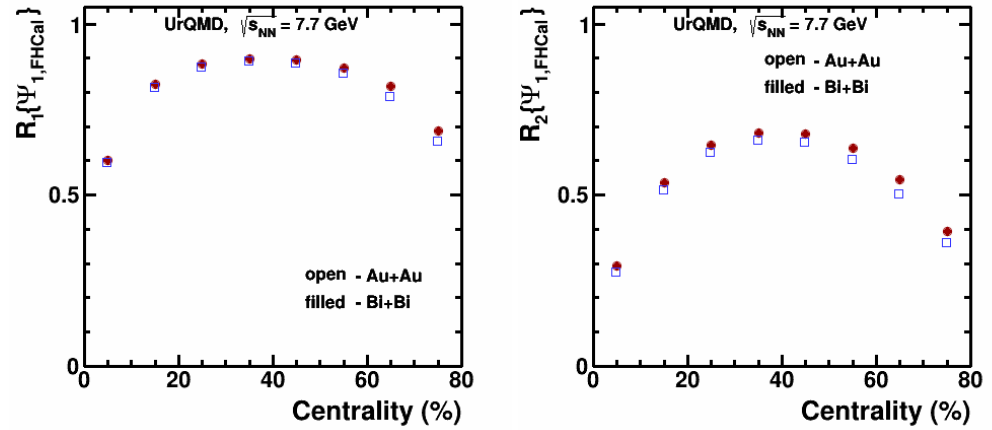


**Figure 7.** Centrality dependence of event plane resolution factors  $R_n(\Psi_{1,\text{FHCal}})$  for the directed  $v_1$  (left) and elliptic  $v_2$  (right) flow measurements for the Au + Au (open symbols) and Bi + Bi (filled symbols) collisions at  $\sqrt{s_{\text{NN}}} = 7.7$  GeV.

For  $V^0$  particles, like  $K_s^0$  and  $\Lambda$ , the  $v_n^{SB}$  of the selected sample contains both  $v_n^S$  of the signal and the  $v_n^B$  of the combinatorial background. The invariant mass ( $M_{\text{inv}}$ ) fit method [22] was applied to extract the anisotropic flow values  $v_n^S$  for  $V^0$  particles. Therefore, the  $v_n^{SB} = \langle \cos[n(\varphi^{\text{pair}} - \Psi_{1,\text{FHCal}})] \rangle$  is measured as a function of invariant mass ( $M_{\text{inv}}$ ) and  $p_T^{\text{pair}}$ :

$$v_n^{SB}(M_{\text{inv}}, p_T^{\text{pair}}) = v_n^S(p_T^{\text{pair}}) \frac{N^S(M_{\text{inv}}, p_T^{\text{pair}})}{N^{SB}(M_{\text{inv}}, p_T^{\text{pair}})} + v_n^B(M_{\text{inv}}, p_T^{\text{pair}}) \frac{N^B(M_{\text{inv}}, p_T^{\text{pair}})}{N^{SB}(M_{\text{inv}}, p_T^{\text{pair}})}, \quad (4)$$

where  $N^S(M_{\text{inv}}, p_T^{\text{pair}})$ ,  $N^B(M_{\text{inv}}, p_T^{\text{pair}})$  and  $N^{SB}(M_{\text{inv}}, p_T^{\text{pair}})$  are signal, background and total yields obtained for each  $p_T^{\text{pair}}$  interval from fits to the  $K_s^0$  and  $\Lambda$  invariant mass distributions, see Figure 5. Values for  $v_n^S$  signal for  $K_s^0$  and  $\Lambda$  particles were extracted via a direct fit to the  $v_n^{SB}(M_{\text{inv}})$  for each  $p_T^{\text{pair}}$  selection by Equation (4). That is, the background  $v_n^B(M_{\text{inv}})$  was parametrized as a linear or quadratic function of  $M_{\text{inv}}$  (depending on the  $p_T^{\text{pair}}$  selection) and  $v_n^S$  is taken as a fit parameter. The accuracy of the extraction procedure was verified by checking that the invariant mass ( $M_{\text{inv}}$ ) dependencies of the sine coefficients  $v_{\sin,n}^{SB} = \langle \sin[n(\varphi^{\text{pair}} - \Psi_{1,\text{FHCal}})] \rangle$ , were all equal to zero within statistical errors. As an example, Figure 8 shows the demonstration of the invariant mass fit method to extract the  $v_1^S$  and  $v_2^S$  signals for  $K_s^0$  (upper part) and  $\Lambda$  (lower part) particles for 10–40% central Au + Au collisions at  $\sqrt{s_{\text{NN}}} = 11$  GeV.

The  $v_n$  results obtained by the event plane analysis can be affected by non-flow and flow fluctuations [4]. The non-flow effects are mainly due to few particle correlations not associated with the reaction plane: Bose–Einstein correlations, resonance decays, momentum conservation and di-jets. In the present study, the large rapidity gap  $\Delta\eta > 0.5$  between the particles detected in TPC and the particles in FHCal reduces the influence of possible non-flow contributions. The elliptic flow results  $v_2^{\Psi_{1,\text{FHCal}}}$  obtained with respect to the spectator first-order event plane are expected to be less affected by the elliptic flow fluctuations because of the strong correlation between the  $\Psi_{1,\text{FHCal}}$  and the true reaction plane  $\Psi_{\text{RP}}$ .

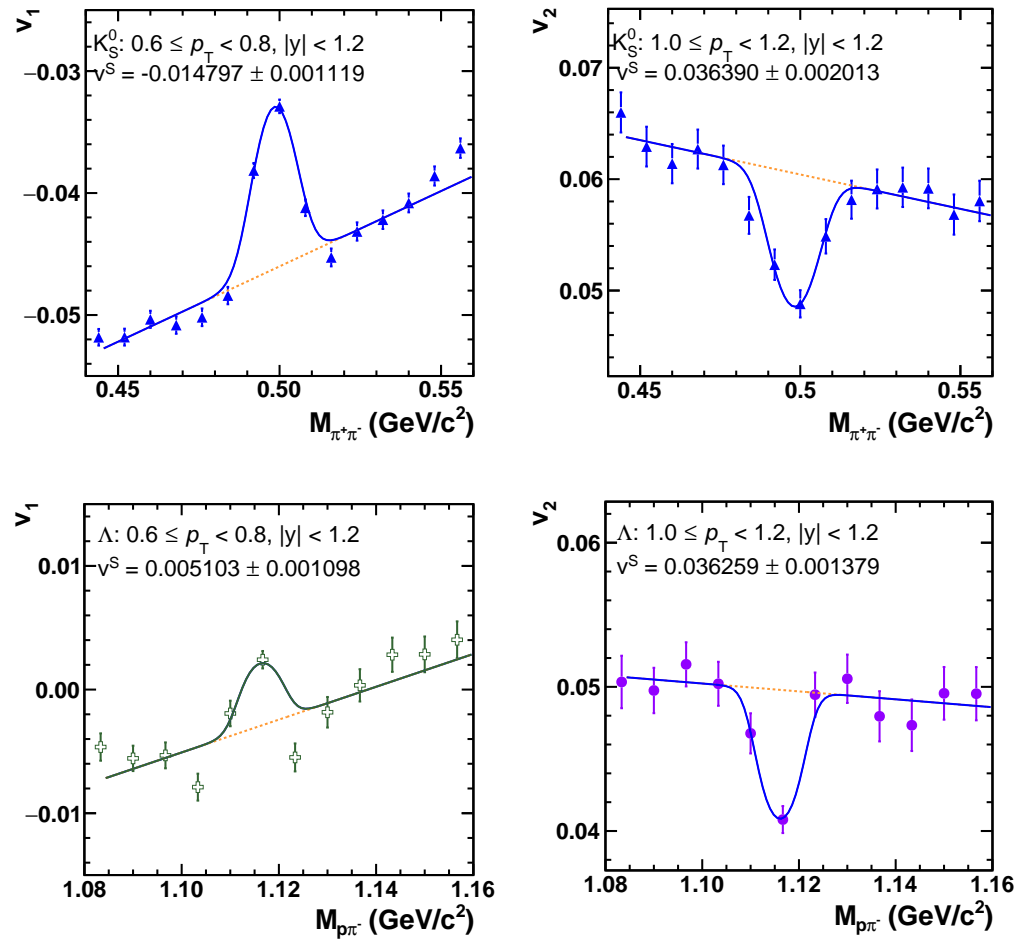


**Figure 8.** The demonstration of the invariant-mass fit method to extract the  $v_1^S$  (left panels) and  $v_2^S$  (right panels) signals for  $K_S^0$  (upper part) and  $\Lambda$  (lower part) particles for 10–40% central Au + Au collisions at  $\sqrt{s_{NN}} = 11$  GeV.

#### 4. Results

Figure 9 presents the rapidity dependence of directed  $v_1(y)$  of charged pions, kaons and protons from Au + Au collisions at  $\sqrt{s_{NN}} = 4.5, 7.7$  and 11 GeV. The left part of the Figure shows the results for 0–10% central collisions and right part for 10–40% central Au + Au collisions.

For all particle species, the directed flow crosses 0 at midrapidity. The reconstructed values “reco” of the directed flow are fully consistent with the generated “true” values in all centrality classes and collision energies. The  $v_1$  and  $v_2$  for identified charged hadrons as a function of transverse momentum  $p_T$  are presented in Figure 10 for 10–40% central Au + Au collisions at  $\sqrt{s_{NN}} = 4.5, 7.7$  and 11 GeV.

The open symbols correspond to  $v_n$  results from the analysis of the fully reconstructed events “reco” and closed symbols and to the results from the generated “true” UrQMD events. The available statistics of 20 M minimum-bias events have allowed us to perform the detailed  $p_T$ -differential measurements of charged pions, kaons and protons up to 1.5 GeV/c. The more detailed  $p_T$ -differential studies as a function of centrality and rapidity will require a larger data sample of up to 300 M of minimum-bias events.

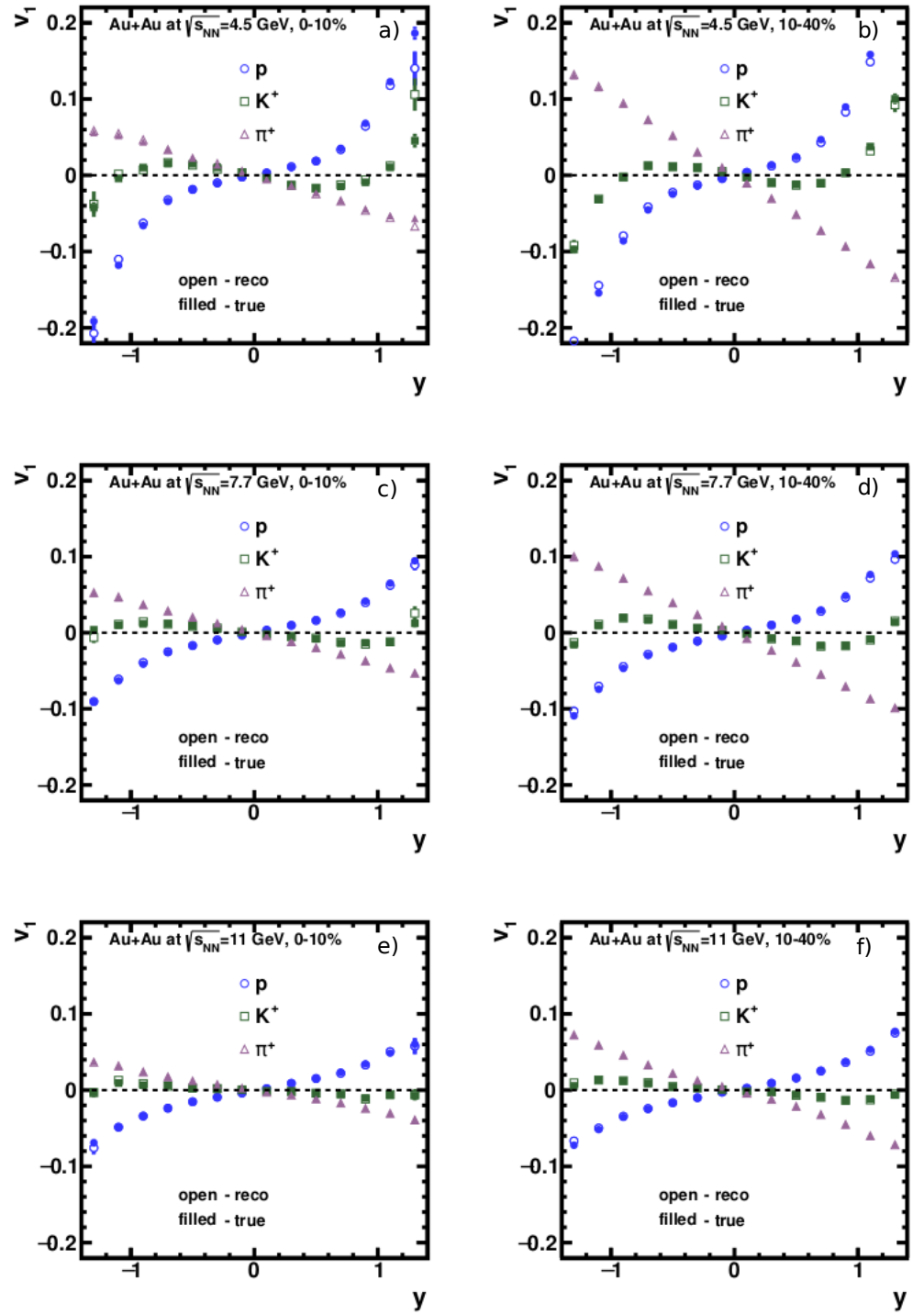


**Figure 9.** Rapidity  $y$  dependence of directed  $v_1$  of charged pions, kaons and protons for 0–10% central (left panels) and 10–40% central (right panels) Au + Au collisions at  $\sqrt{s_{NN}} = 4.5, 7.7$  and 11 GeV. The open symbols correspond to  $v_1$  results from the analysis of the fully reconstructed events “reco” and closed symbols to the results from generated “true” UrQMD events.

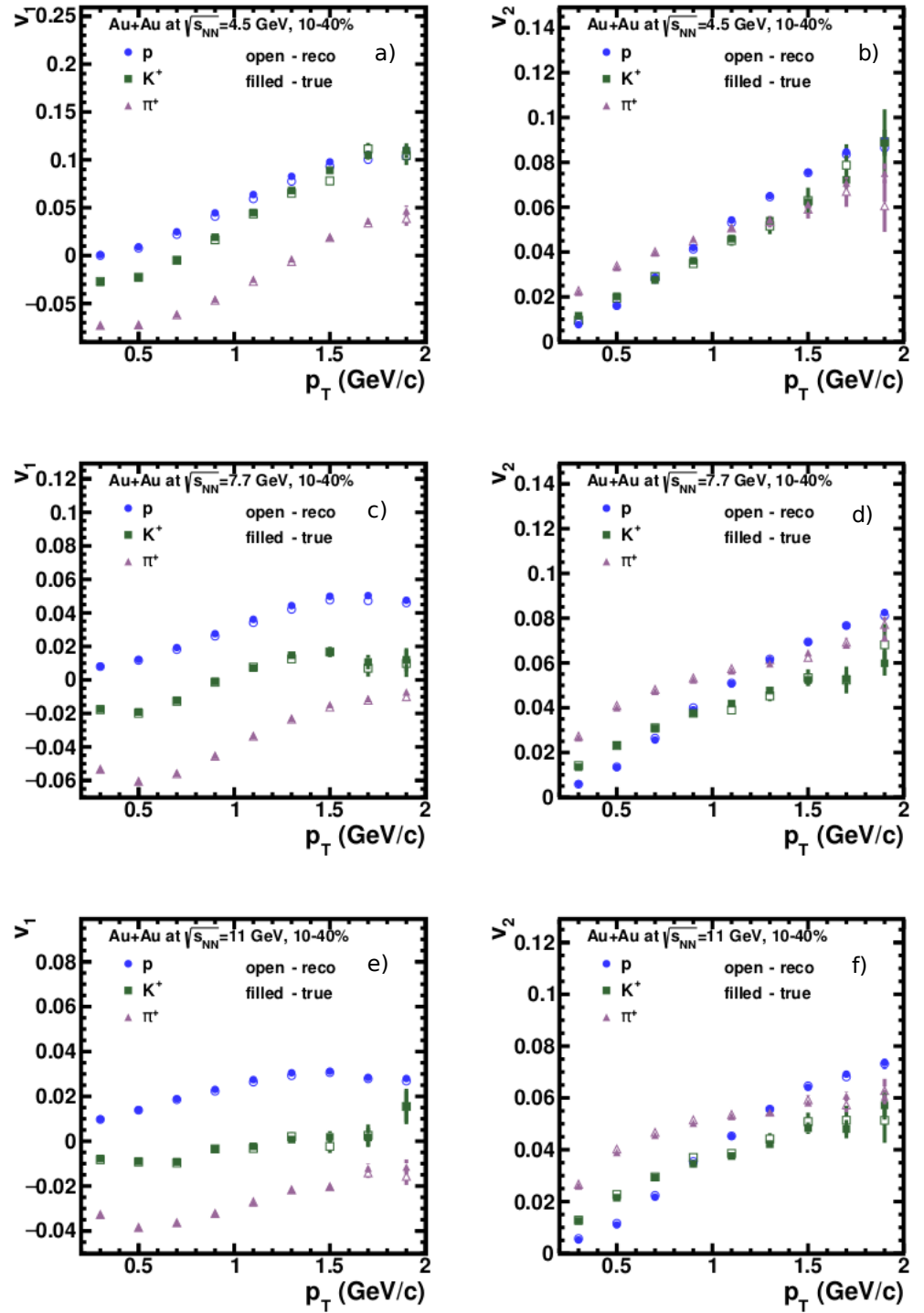


**Figure 10.**  $p_T$  dependence of directed  $v_1$  (left panels) and elliptic  $v_2$  flow (right panels) of charged pions, kaons and protons for 10–40% central Au + Au collisions at  $\sqrt{s_{NN}} = 4.5, 7.7$  and 11 GeV. The open symbols correspond to  $v_n$  results from the analysis of the fully reconstructed events ("reco") and closed symbols to the results from generated ("true") UrQMD events.

Figures 11 and 12 illustrate the MPD detector system performance for the differential directed  $v_1(y)$  and elliptic flow measurements  $v_2(p_T)$  of  $K_S^0$  and  $\Lambda$  particles for 10–40% central Au + Au collisions at  $\sqrt{s_{NN}} = 11$  GeV. The results were obtained from the analysis of 25 M minimum-bias fully reconstructed UrQMD events. A good agreement is observed between the  $v_n$  results of  $K_S^0$  and  $\Lambda$  particles extracted by invariant-mass fit method illustrated in the Figure 8 from the fully reconstructed data “reco” and generated “true” UrQMD events.

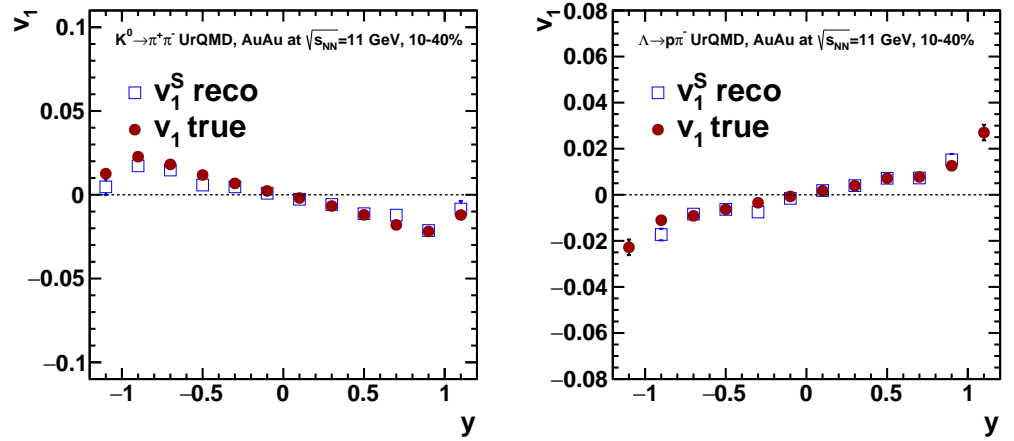


**Figure 11.** Rapidity  $y$  dependence of directed  $v_1$  flow of  $K_S^0$  (left) and  $\Lambda$  (right) particles for 10–40% central Au + Au collisions at  $\sqrt{s_{NN}} = 11$  GeV: open symbols represent the “true”  $v_2$  results and filled symbols the “reco”  $v_2$  results.

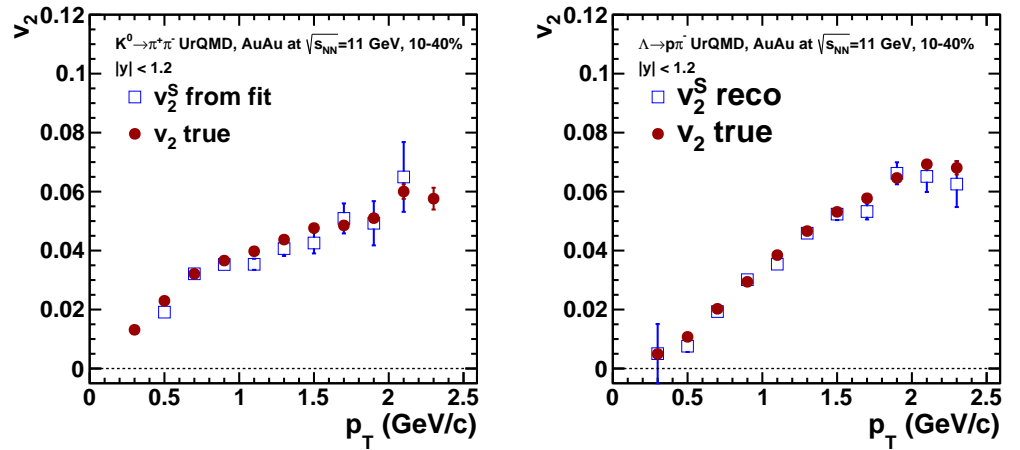


**Figure 12.**  $p_T$  dependence of  $v_2\{\Psi_{1,FHCal}\}$  of  $K_S^0$  (left) and  $\Lambda$  (right) particles for 10–40% central Au + Au collisions at  $\sqrt{s_{NN}} = 11$  GeV: open symbols represent the “true”  $v_2$  results and filled symbols the “reco”  $v_2$  results.

The final part of this study is related to the comparison of the differential  $v_1$  and  $v_2$  results of identified hadrons from two colliding systems Au + Au and Bi + Bi at  $\sqrt{s_{NN}} = 7.7$  GeV. The NICA collider is planned to start with first beams of  $^{209}\text{Bi}$  ions in 2023. The delivery of  $^{198}\text{Au}$  ions will be accomplished after this phase of NICA operation. Figure 13 presents the detailed comparison of the differential  $v_1(y)$  results for charged pions and protons for 0–10% central (left panels) and 10–40% central (right panels) Au + Au and Bi + Bi collisions at  $\sqrt{s_{NN}} = 7.7$  GeV. The  $v_1(y)$  results have been obtained from the event plane analysis of 30 M fully reconstructed minimum-bias UrQMD events. The results received for Au + Au (Bi + Bi) collisions are marked as open (filled) symbols. Figure 14 shows the performance of measuring the  $p_T$  dependence of directed  $v_1$  (left) and

elliptic  $v_2$  (right) flow coefficients of charged pions and protons for 10–40% central Au + Au (open symbols) and Bi + Bi (filled symbols) collisions. The expected small difference is observed in the  $v_n$  results for two colliding systems.

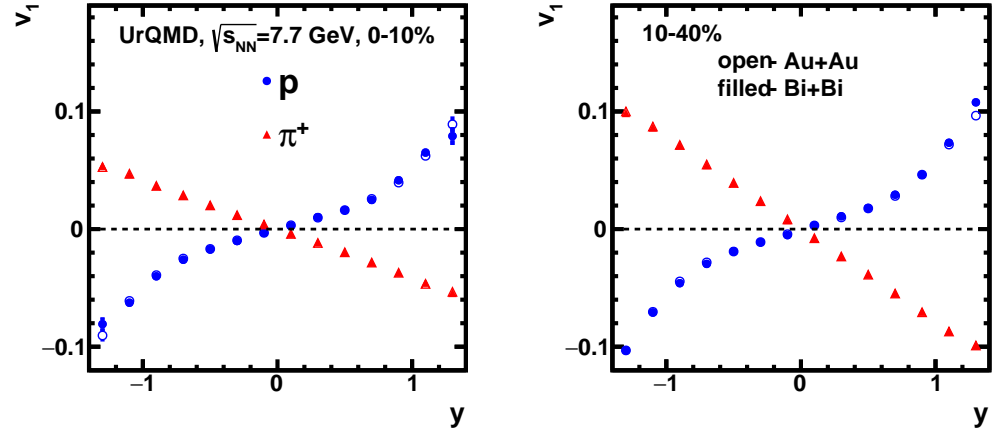


**Figure 13.** Rapidity  $y$  dependence of directed  $v_1$  flow of charged pions and protons for 0–10% central (left panel) and 10–40% central (right panel) collisions at  $\sqrt{s_{NN}} = 7.7$  GeV. Open symbols represent results for Au + Au and closed symbols for Bi + Bi collisions.

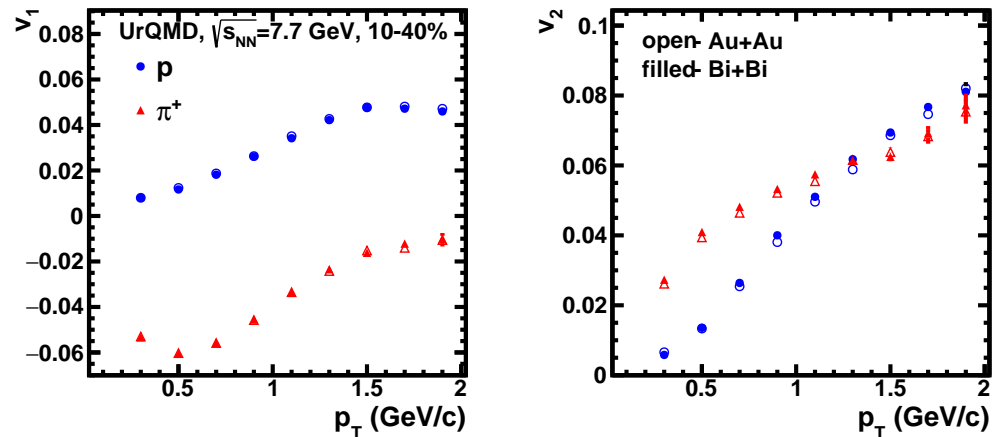


**Figure 14.**  $p_T$  dependence of directed  $v_1$  flow (left panel) and elliptic flow  $v_2$  (right panel) of charged pions and protons for 10–40% central heavy-ion collisions at  $\sqrt{s_{NN}} = 7.7$  GeV. Open symbols represent results for Au + Au and closed symbols for Bi + Bi collisions.

## 5. Conclusions

In this work, the performance of the MPD experiment for directed ( $v_1$ ) and elliptic ( $v_2$ ) flow measurements was studied with Monte Carlo simulations using  $^{198}\text{Au} + ^{198}\text{Au}$  and  $^{209}\text{Bi} + ^{209}\text{Bi}$  collisions at NICA energies. A large sample of generated UrQMD minimum bias events has been used as an input for the full chain of realistic simulations of the MPD detector subsystems based on the GEANT4 platform and reconstruction algorithms built in the MPDROOT. Realistic procedures for centrality determination, particle identification and event plane reconstruction have been used in the analysis. The resulting performance of the MPD has been verified for  $v_1$  and  $v_2$  measurements of identified charged pions, kaons, protons,  $K_s^0$  and  $\Lambda$  particles as a function of rapidity and transverse momentum in different centrality classes. The detailed comparison of the results obtained from the analysis of the fully reconstructed data and generator-level data has allowed us to conclude that MPD system will provide the detailed differential measurements of directed and elliptic flows

with high efficiency. In future we plan to include the data from other transport models [23] and extend the study to other colliding systems.

**Author Contributions:** All authors contributed equally to this work. All authors have read and agreed to the published version of the manuscript.

**Funding:** This research was funded by the RFBR according to the research project No. 18-02-40086 and partially supported by the European Union’s Horizon 2020 research and innovation program under grant agreement No. 871072 and by the Ministry of Science and Higher Education of the Russian Federation, Project “Fundamental properties of elementary particles and cosmology” No 0723-2020-0041.

**Acknowledgments:** The authors thank Alexander Zinchenko and Alexander Mudrokh for helpful discussions and comments. We thank Andrey Moshkin from the MPD collaboration for the help with production of the reconstructed data used in the analysis. Computational resources were provided by the NRNU MEPhI high-performance computing center and NICA high-performance cluster of LHEP JINR.

**Conflicts of Interest:** The authors declare no conflict of interest. The funders had no role in the design of the study; in the collection, analyses, or interpretation of data; in the writing of the manuscript, or in the decision to publish the results.

## References

1. Kekelidze, V.D. Heavy Ion Collisions: Baryon Density Frontier. *Phys. Part. Nucl.* **2018**, *49*, 457. [\[CrossRef\]](#) [\[CrossRef\]](#)
2. Golovatyuk, V.; Kekelidze, V.; Kolesnikov, V.; Rogachevsky, O.; Sorin, A. The Multi-Purpose Detector (MPD) of the collider experiment. *Eur. Phys. J. A* **2016**, *52*, 212. [\[CrossRef\]](#) [\[CrossRef\]](#)
3. Kisiel, A. [MPD] Status of the MPD Experiment at JINR. *J. Phys. Conf. Ser.* **2020**, *1602*, 012021. [\[CrossRef\]](#) [\[CrossRef\]](#)
4. Voloshin, S.A.; Poskanzer, A.M.; Snellings, R. Collective phenomena in non-central nuclear collisions. *Landolt-Bornstein* **2010**, *23*, 293. [\[CrossRef\]](#)
5. Bernhard, J.E.; Moreland, J.S.; Bass, S.A. Bayesian estimation of the specific shear and bulk viscosity of quark-gluon plasma. *Nature Phys.* **2019**, *15*, 1113–1117. [\[CrossRef\]](#) [\[CrossRef\]](#)
6. Adamczyk, L.; Adkins, J.K.; Agakishiev, G.; Aggarwal, M.M.; Ahammed, Z.; Alekseev, I.; Alford, J.; Anson, C.D.; Aparin, A.; Arkhipkin, D.; et al. Beam-Energy Dependence of the Directed Flow of Protons, Antiprotons, and Pions in Au + Au Collisions. *Phys. Rev. Lett.* **2014**, *112*, 162301. [\[CrossRef\]](#) [\[CrossRef\]](#) [\[PubMed\]](#)
7. Adamczyk, L.; Adams, J.R.; Adkins, J.K.; Agakishiev, G.; Aggarwal, M.M.; Ahammed, Z.; Ajitanand, N.N.; Alekseev, I.; Anderson, D.M.; Aoyama, R.; et al. Beam-Energy Dependence of Directed Flow of  $\Lambda$ ,  $\bar{\Lambda}$ ,  $K^\pm$ ,  $K_s^0$  and  $\phi$  in Au + Au Collisions. *Phys. Rev. Lett.* **2018**, *120*, 062301. [\[CrossRef\]](#) [\[CrossRef\]](#) [\[PubMed\]](#)
8. Adamczyk, L.; Adamczyk, L.; Adkins, J.K.; Agakishiev, G.; Aggarwal, M.M.; Ahammed, Z.; Alekseev, I.; Alford, J.; Anson, C.D.; Aparin, A.; et al. Elliptic flow of identified hadrons in Au + Au collisions at  $\sqrt{s_{NN}} = 7.7\text{--}62.4$  GeV. *Phys. Rev. C* **2013**, *88*, 014902. [\[CrossRef\]](#) [\[CrossRef\]](#)
9. Adamczyk, L.; Agakishiev, G.; Aggarwal, M.M.; Ahammed, Z.; Alakhverdyants, A.V.; Alekseev, I.; Alford, J.; Anderson, B.D.; Anson, C.D.; Arkhipkin, D.; et al. Inclusive charged hadron elliptic flow in Au + Au collisions at  $\sqrt{s_{NN}} = 7.7\text{--}39$  GeV. *Phys. Rev. C* **2012**, *86*, 054908. [\[CrossRef\]](#) [\[CrossRef\]](#)
10. Kashirin, E.; Selyuzhenkov, I.; Golosov, O.; Klochov, V.; NA49 and NA61/SHINE. Anisotropic Flow Measurements from the NA61/SHINE and NA49 Beam Momentum Scan Programs at CERN SPS. *Phys. Part. Nucl.* **2020**, *51*, 301–304. [\[CrossRef\]](#) [\[CrossRef\]](#)
11. Pinkenburg, C.; Ajitanand, N.N.; Alexander, J.M.; Anderson, M.; Best, D.; Brady, F.P.; Case, T.; Caskey, W.; Cebra, D.; Chance, J.L.; et al. Elliptic flow: Transition from out-of-plane to in-plane emission in Au + Au collisions. *Phys. Rev. Lett.* **1999**, *83*, 1295–1298. [\[CrossRef\]](#) [\[CrossRef\]](#)
12. Liu, H.; Ajitanand, N.N.; Alexander, J.M.; Anderson, M.; Best, D.; Brady, F.P.; Case, T.; Caskey, W.; Cebra, D.; Chance, J.; et al. Sideward flow in Au + Au collisions between 2-A-GeV and 8-A-GeV. *Phys. Rev. Lett.* **2000**, *84*, 5488–5492. [\[CrossRef\]](#) [\[CrossRef\]](#) [\[PubMed\]](#)
13. Adamczewski-Musch, J.; Arnold, O.; Behnke, C.; Belounnas, A.; Belyaev, A.; Berger-Chen, J.C.; Blanco, A.; Blume, C.; Bohmer, M.; Bordalo, P.; et al. Directed, Elliptic, and Higher Order Flow Harmonics of Protons, Deuterons, and Tritons in Au + Au Collisions at  $\sqrt{s_{NN}} = 2.4$  GeV. *Phys. Rev. Lett.* **2020**, *125*, 262301. [\[CrossRef\]](#) [\[CrossRef\]](#) [\[PubMed\]](#)
14. Taranenko, A. Anisotropic flow measurements from RHIC to SIS. *EPJ Web Conf.* **2019**, *204*, 03009. [\[CrossRef\]](#) [\[CrossRef\]](#)
15. Bleicher, M.; Zabrodin, E.; Spieles, C.; Bass, S.A.; Ernst, C.; Soff, S.; Bravina, L.; Belkacem, M.; Weber, H.; Stoecker, H.; et al. Relativistic hadron hadron collisions in the ultrarelativistic quantum molecular dynamics model. *J. Phys. G* **1999**, *25*, 1859–1896. [\[CrossRef\]](#) [\[CrossRef\]](#)

16. Bass, S.A.; Belkacem, M.; Bleicher, M.; Brandstetter, M.; Bravina, L.; Ernst, C.; Gerland, L.; Hofmann, M.; Hofmann, S.; Konopka, J.; et al. Microscopic models for ultrarelativistic heavy ion collisions. *Prog. Part. Nucl. Phys.* **1998**, *41*, 255–369. [\[CrossRef\]](#) [\[CrossRef\]](#)
17. Agostinelli, S.; Allison, J.; Amako, K.A.; Apostolakis, J.; Araujo, H.; Arce, P.; Asai, M.; Axen, D.; Banerjee, S.; Barrand, G.; et al. GEANT4—a simulation toolkit. *Nucl. Instrum. Meth. A* **2003**, *506*, 250–303. [\[CrossRef\]](#) [\[CrossRef\]](#)
18. Kolesnikov, V.; Mudrokh, A.; Vasendina, V.; Zinchenko, A. Towards a Realistic Monte Carlo Simulation of the MPD Detector at NICA. *Phys. Part. Nucl. Lett.* **2019**, *16*, 6–15. [\[CrossRef\]](#) [\[CrossRef\]](#)
19. Loizides, C.; Nagle, J.; Steinberg, P. Improved version of the PHOBOS Glauber Monte Carlo. *SoftwareX* **2015**, *1–2*, 13–18. [\[CrossRef\]](#) [\[CrossRef\]](#)
20. Zinchenko, A.; Kolesnikov, V.; Mudrokh, A.; Vasendina, V.; Voronyuk, V. Prospects for the study of the strangeness and hypernuclei production at NICA/MPD. *J. Phys. Conf. Ser.* **2019**, *1390*, 012017. [\[CrossRef\]](#) [\[CrossRef\]](#)
21. Poskanzer, A.M.; Voloshin, S.A. Methods for analyzing anisotropic flow in relativistic nuclear collisions. *Phys. Rev. C* **1998**, *58*, 1671. [\[CrossRef\]](#) [\[CrossRef\]](#)
22. Borghini, N.; Ollitrault, J.Y. Azimuthally sensitive correlations in nucleus-nucleus collisions. *Phys. Rev. C* **2004**, *70*, 064905. [\[CrossRef\]](#) [\[CrossRef\]](#)
23. Parfenov, P.; Taranenko, A.; Idrisov, D.; Luong, V.B.; Geraksiev, N.; Demanov, A.; Povarov, A.; Kireyeu, V.; Truttse, A.; Volodihin, E. The comparison of methods for anisotropic flow measurements with the MPD Experiment at NICA. *arXiv* **2020**, arXiv:2012.06763.